SF2A 2013
L. Cambrésy, F. Martins, E. Nuss and A. Palacios (eds)

PROPERTIES OF INTERSTELLAR FILAMENTS OBSERVED WITH *HERSCHEL* : WHAT CAN WE SAY ABOUT THEIR FORMATION AND EVOLUTION?

D. Arzoumanian[1], Ph. André[2], N. Peretto[3], V. Könyves[1,2] and P. Palmeirim[2]

Abstract. We present a scenario for filament formation and evolution motivated by recent observational results of nearby molecular clouds. The analysis of more than 270 filaments observed in 8 regions by the *Herschel* Gould Belt survey show that the filaments are characterized by a narrow distribution of central width sharply peaked at ∼0.1 pc. This typical filament width corresponds, within a factor of ∼ 2 to the sonic scale below which interstellar turbulence becomes subsonic, which may suggest that the filaments form as a result of the dissipation of large-scale turbulence. The analysis of IRAM 30m molecular line observations of a sample of these filaments show evidence of an increase in non-thermal velocity dispersion with column density which suggest an evolution of the supercritical filaments in mass per unit length while accreting surrounding material. Relative orientations of magnetic field lines and filamentary structures indicate that interstellar magnetic fields may play an important role in shaping the structure of, at least, some molecular clouds and help in channeling low-density material onto star forming filaments.

Keywords: ISM, star formation, interstellar filament formation and evolution, magnetic fields

1 Omnipresence of filaments in molecular clouds

Interstellar filaments have recently received special attention, thanks to the high quality and dynamic range of *Herschel* observations. While molecular clouds (MC) were already known to exhibit filamentary structures (cf. Schneider & Elmegreen 1979), *Herschel* observations revealed the omnipresence of the filaments in the galaxy (e.g., André et al. 2010; Molinari et al. 2010; Schneider et al. 2012). Recent results from the *Herschel* Gould Belt survey (HGBS) showed that most of the prestellar cores are located within gravitationally unstable filaments for which the mass per unit length exceeds the critical value $M_{\rm line} > M_{\rm line,crit} = 2\,c_s^2/G \sim 16\,M_\odot$/pc (Ostriker 1964), where $c_{\rm s} \sim 0.2$ km/s is the isothermal sound speed for $T \sim 10$ K, while the subcritical filaments for which $M_{\rm line} < M_{\rm line,crit}$ are devoid of any bound cores (André et al. 2010; Arzoumanian et al. 2011; Palmeirim et al. 2013). This early result suggests an intimate connection between the filamentary structure and the formation process of prestellar cores and protostars. Statistical analysis of the filaments is now possible thanks to the resolution and sensitivity of *Herschel* (Pilbratt et al. 2010) SPIRE (Griffin et al. 2010) and PACS (Poglitsch et al. 2010) observations which are ideal to characterize the properties of the filamentary structure and investigate the physical processes involved in their formation and evolution.

2 A characteristic width for interstellar filaments revealed by *Herschel*

A sample of 278 filaments observed by the HGBS were extracted and analyzed. Mean radial column density profiles for each filament were derived from the column density maps constructed from *Herschel* images (as explained in Könyves et al. 2010; Palmeirim et al. 2013). The constructed column density radial profiles were modeled with a Plummer-like function (cf. Arzoumanian et al. 2011). The observed density profiles of the filaments approach a power law, at large radii with $\rho(r) \sim r^{-2}$ (Arzoumanian et al. 2011; Hill et al. 2012; Palmeirim et al. 2013), and none of them shows the steep density profile of the Ostriker (1964) model of an isothermal filament in hydrostatic equilibrium, for which $\rho(r) \sim r^{-4}$. Masses per unit length of the filaments were derived by integrating the column density profiles over radius $M_{\rm line}^{\rm obs} = \int \Sigma_{\rm obs}(r) {\rm d}r$.

[1] IAS, CNRS (UMR 8617), Universit Paris-Sud, Btiment 121, 91400 Orsay, France
[2] Laboratoire AIM, CEA/DSM–CNRS–Université Paris Diderot, IRFU/Service d'Astrophysique, C.E.A. Saclay, Orme des Merisiers, 91191 Gif-sur-Yvette, France
[3] School of Physics & Astronomy, Cardiff University, Queens Buildings, The parade, Cardiff CF24 3AA, UK

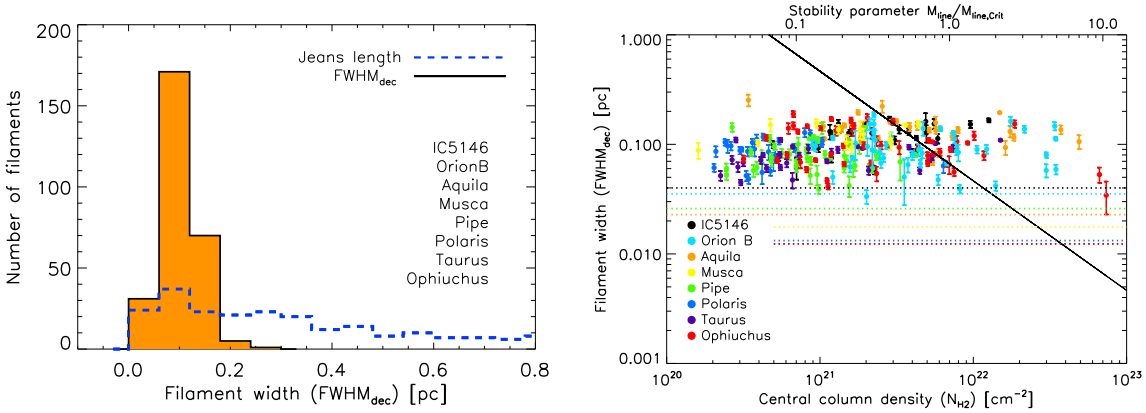

Fig. 1. Left: Distribution of deconvolved FWHM widths for the 278 filaments (black solid histogram, filled in orange), with a median value of 0.09 pc and a standard deviation of 0.04 pc. For comparison, the blue dashed histogram represents the distribution of central Jeans lengths corresponding to the central column densities of the filaments [$\lambda_J = c_s^2/(G\Sigma_0)$] for T = 10 K. **Right**: Mean deconvolved width versus background subtracted central column density for the same filament sample. The spatial resolutions of the column density maps used in the analysis for the different regions are marked by the horizontal dotted lines. The solid line running from top left to bottom right shows the central (thermal) Jeans length as a function of central column density. The upper x-axis scale corresponds to an estimation of the mass per unit length of the filaments in units of the thermal critical line mass, where $M_{\rm line} = W\Sigma_0$ with W = 0.1 pc and $M_{\rm line,crit} = 2c_s^2/G$ (improved versions of Fig. 6 and 7 from Arzoumanian et al. 2011).

The filament central widths were measured from Gaussian fits to the radial column density profiles. The analyzed filaments have a narrow distribution of FWHM widths centred around a typical value of 0.09 ± 0.04 pc (Fig. 1–left). The same filaments, observed in 8 regions (listed in Fig. 1) located at distances from 140 pc to 460 pc, span more than three orders of magnitude in central column density (Fig. 1–right) implying a distribution of central Jeans lengths from 0.02 pc up to 1.3 pc, which is much broader than the observed distribution of widths.

3 Proposed scenario for filament formation and evolution

We complemented the analysis of filament properties derived from *Herschel* imaging data with molecular line observations to gain insight into the gas kinematics of interstellar filaments. We used $C^{18}O$ and N_2H^+ line observations obtained with the IRAM 30m telescope to measure the velocity dispersions of a sample of filaments detected as part of the *Herschel* Gould Belt Survey in the IC5146, Aquila, and Polaris interstellar clouds (Arzoumanian et al. 2013).

Correlating the velocity dispersion measurements with the filament column densities derived from *Herschel* data, we see that interstellar filaments can be divided into two groups: thermally subcritical filaments, which have transonic velocity dispersions ($c_s \lesssim \sigma_{tot} < 2\,c_s$) independent of column density; and thermally supercritical filaments, which have higher velocity dispersions scaling roughly as the square root of column density ($\sigma_{tot} \propto \Sigma^{0.5}$). Assuming that the filaments have Gaussian radial column density profiles an estimated filament mass per unit length is given by $M_{\rm line} \sim \Sigma_0 \times W_{\rm fil}$ where $W_{\rm fil} \sim 0.1$ pc is the typical filament width (Arzoumanian et al. 2011). Interestingly, the observationally estimated $M_{\rm line}^{\rm threshold}$ for the column density threshold $\sim 8\times10^{21}$ cm^{-2}, which seems to divide the filament sample into two groups (cf. Fig. 2), is equal within a factor of ~2 to the theoretical $M_{\rm line,crit} \sim 16$ M$_\odot$/pc (for T=10 K). Thereby, the filament $M_{\rm line,crit}$ corresponds to a column density boundary, where subcritical filaments (left hand side of the boundary) have roughly constant velocity dispersions with a mean value of (0.26 ± 0.05) km/s, while the velocity dispersions of supercritical filaments (right hand side of the boundary) increase as a function of projected column density $\sigma_{\rm tot} \propto {N_{H_2}}^{0.5}$. Moreover, the filament virial line masses $M_{\rm line,vir} = 2\,\sigma_{\rm tot}^2/G$ (replacing $M_{\rm line,crit}$ in the presence of nonthermal motions – see Fiege & Pudritz 2000), show that thermally supercritical filaments are in approximate virial balance, while thermally subcritical filaments are unbound (Arzoumanian et al. 2013). This result shows that the gravitational stability criterion, based on the thermal critical line mass, assuming that the filaments have thermally dominated velocity dispersions (André et al. 2010), is consistent with a more complete view of the total velocity dispersion of filaments.

The observational evidence of a characteristic filament width may be consistent with a scenario for filament formation from dissipation of large-scale supersonic interstellar turbulence (Padoan et al. 2001). In such a picture, filaments coincide with stagnation gas associated with regions of locally converging turbulent motions, where compression is at a maximum

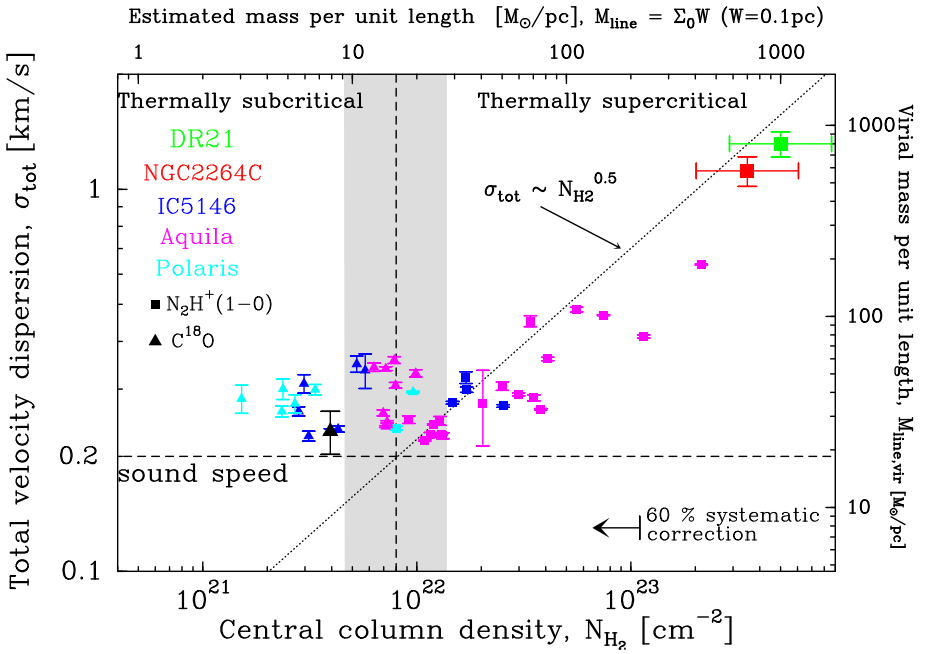

Fig. 2. Total velocity dispersion versus observed central column density: blue for IC5146, magenta for Aquila, cyan for Polaris, red for NGC2264C, and green for DR21 filaments. The horizontal dashed line shows the value of the sound speed ~ 0.2 km/s for T=10 K. The vertical dashed line marks the boundary between thermally subcritical and thermally supercritical filaments where the estimated mass per unit length $M_{\rm line}$ is approximately equal to the critical value $M_{\rm line,crit} \sim 16\ {\rm M}_\odot$/pc for T=10 K, equivalent to a column density of 8×10^{21} cm^{-2}. The grey band shows a dispersion of a factor of 3 around this nominal value. The dotted line running from the bottom left to the top right corresponds to $\sigma_{\rm tot} \propto {\rm N_{H_2}}^{0.5}$ (cf. Arzoumanian et al. 2013).

and relative velocity differences at a minimum, and are thus expected to have relatively low (transonic) internal velocity dispersions (cf. Klessen et al. 2005). The line-of-sight velocity dispersions measured here for subcritical filaments are consistent with this picture. The typical filament width would correspond to the dissipation scale of the ion-neutral friction in the ISM as suggested by Hennebelle (2013). While the turbulent picture provides a plausible mechanism for *forming* the filaments, the fact that prestellar cores tend to form in gravitationally unstable filaments suggests that gravity is a major driver in the subsequent *evolution* of the supercritical, self gravitating filaments. The higher velocity dispersions of supercritical filaments may not directly arise from supersonic interstellar turbulence but may be driven by gravitational contraction/accretion (cf. Klessen & Hennebelle 2010). The accretion driven turbulence in supercritical filaments has been supported by numerical simulations of Heitsch (2013).

Based on our observational results, we propose an evolutionary scenario whereby supercritical filaments undergo gravitational contraction and increase in mass per unit length through accretion of background material while remaining in rough virial balance. We further suggest that this accretion process allows supercritical filaments to keep their approximately constant inner widths (0.1 pc) while contracting (Arzoumanian et al. 2013).

4 Role of interstellar magnetic field in the formation and evolution of filamentary structures

This growth in mass per unit length of supercritical filaments by accretion of surrounding material is suggested by low-density striations or subfilaments observed connected perpendicularly to the main filaments and apparently feeding them from the side. Examples include the B211/B213 filament in Taurus where the typical velocities expected for the infalling material are consistent with the existing kinematical constraints from CO observations (Palmeirim et al. 2013, and see Fig. 3), the Serpens South filament (Könyves et al. 2010; Sugitani et al. 2011), the Musca filament (Pereyra & Magalhães 2004), and the DR21 ridge in Cygnus X (Schneider et al. 2010).

The orientation of the striations aligned with optical polarization vectors in the Taurus field (see Fig. 3) suggests that the magnetic field participates in shaping the morphology of the filamentary structure in the cloud and helps channeling low density material onto the supercritical filament in form of low-density striations. This picture is also consistent with observations of near-IR polarization measurements towards the Serpens South filamentary region which reveal a relatively uniform magnetic field perpendicular to the supercritical star-forming filament (Sugitani et al. 2011).

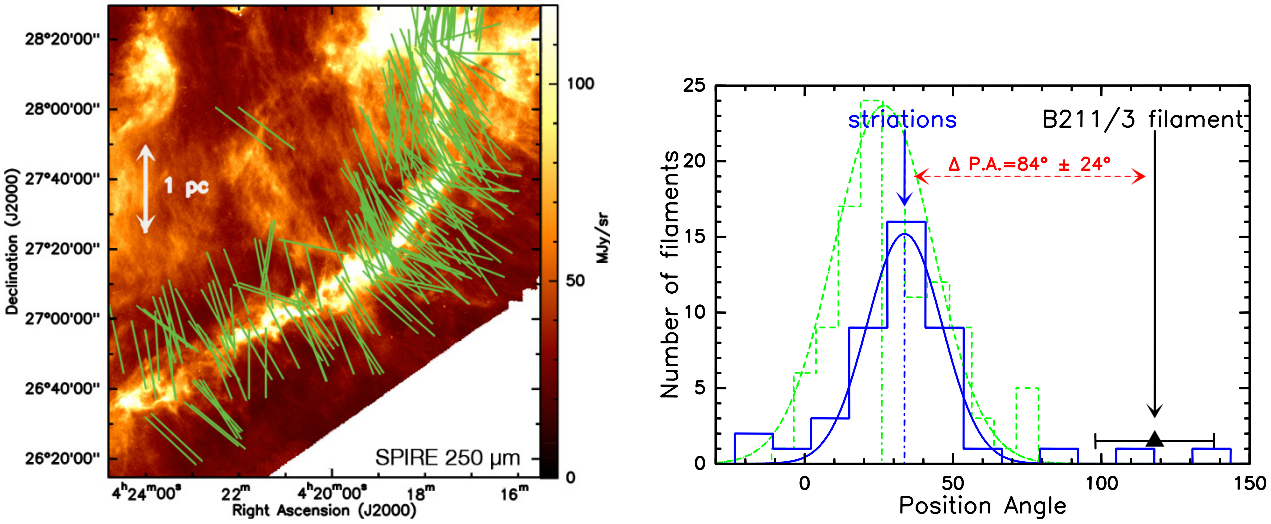

Fig. 3. Left: *Herschel* SPIRE 250 μm image of the Taurus B211/B213 filament and its local cloud. The green segments show the optical and infrared polarization vectors from Heyer et al. (2008); Heiles (2000), and Chapman et al. (2011) tracing the magnetic field orientation. The plane-of-the-sky projection of the magnetic field appears to be oriented perpendicular to the B211/B213 filament and roughly aligned with the general direction of the striations (cf. Palmeirim et al. 2013). **Right**: Orientation of the low-density striations identified in the Taurus field (blue histogram). The position-angle distribution of available optical polarization and infrared vectors are shown by the green dashed histogram. Gaussian fits to these distributions are superimposed, indicating a peak position angle of $34° \pm 13°$ for the striations and $26° \pm 18°$ for the B-field polarization vectors. The B211 filament has a mean position angle of $118° \pm 20°$ (black triangle and horizontal error bar) and is thus roughly perpendicular to both the low-density striations and the local direction of the magnetic field (Fig. 4 from Palmeirim et al. 2013).

These observational results are supported by theoretical arguments which predict that, in the presence of a strong magnetic field, low-density, thermally subcritical filaments should be preferentially oriented parallel to the field lines, while high-density, self-gravitating filaments should be preferentially oriented perpendicular to the field lines (e.g., Nagai et al. 1998). This difference arises because in the presence of a magnetic field, motions of slightly ionized gas do not encounter any resistance along the field lines but encounter significant resistance perpendicular to the field lines. Consequently, an initial perturbation in a low-density part of the cloud will tend to expand along the field lines and form an elongated structure or a subcritical filament parallel to the field. Conversely, a self-gravitating structure will tend to contract along the field lines, forming a condensed, self-gravitating sheet (cf. Nakamura & Li 2008) which can itself fragment into several supercritical filaments oriented perpendicular to the field (e.g. Nagai et al. 1998).

This *bimodal orientation* of molecular structures and filaments has also been noticed in MHD simulations of cloud evolution where dense molecular structures tend to be oriented perpendicular to the magnetic field lines while fainter structures are aligned with the field lines (Soler et al. 2013).

Theoretical considerations, observational results as well as analysis on data performed by numerical simulation seem to agree on the existence of a correlation between the filamentary structure and the configuration of the magnetic field lines in molecular clouds. This suggests that magnetic field may play a role in shaping the morphology of the filamentary clouds and participate in the formation and evolution of interstellar filaments which existence, at least the supercritical ones, appear to be directly connected to the star formation process in molecular clouds.

Acknowledgements. DA acknowledges support by the European Research Council grant MISTIC (ERC-267934)

References

André, P., Men'shchikov, A., Bontemps, S., et al. 2010, A&A, 518, L102+

Arzoumanian, D., André, P., Didelon, P., et al. 2011, A&A, 529, L6

Arzoumanian, D., André, P., Peretto, N., & Könyves, V. 2013, A&A, 553, A119

Chapman, N. L., Goldsmith, P. F., Pineda, J. L., et al. 2011, ApJ, 741, 21

Fiege, J. D. & Pudritz, R. E. 2000, MNRAS, 311, 85

Griffin, M. J., Abergel, A., Abreu, A., et al. 2010, A&A, 518, L3+
Heiles, C. 2000, AJ, 119, 923
Heitsch, F. 2013, ApJ, 769, 115
Hennebelle, P. 2013, A&A, 556, A153
Heyer, M., Gong, H., Ostriker, E., & Brunt, C. 2008, ApJ, 680, 420
Hill, T., Andre, P., Arzoumanian, D., et al. 2012, A&A, 548, L6
Klessen, R. S. & Hennebelle, P. 2010, A&A, 520, A17
Könyves, V., André, P., Men'shchikov, A., et al. 2010, A&A, 518, L106+
Molinari, S., Swinyard, B., Bally, J., et al. 2010, A&A, 518, L100+
Nagai, T., Inutsuka, S.-I., & Miyama, S. M. 1998, ApJ, 506, 306
Nakamura, F. & Li, Z. 2008, ApJ, 687, 354
Ostriker, J. 1964, ApJ, 140, 1056
Padoan, P., Juvela, M., Goodman, A. A., & Nordlund, Å. 2001, ApJ, 553, 227
Palmeirim, P., André, P., Kirk, J., et al. 2013, A&A, 550, A38
Pereyra, A. & Magalhães, A. M. 2004, ApJ, 603, 584
Pilbratt, G. L., Riedinger, J. R., Passvogel, T., et al. 2010, A&A, 518, L1+
Poglitsch, A., Waelkens, C., Geis, N., et al. 2010, A&A, 518, L2+
Schneider, N., Csengeri, T., Bontemps, S., et al. 2010, A&A, 520, A49+
Schneider, N., Csengeri, T., Hennemann, M., et al. 2012, A&A, 540, L11
Schneider, S. & Elmegreen, B. G. 1979, ApJs, 41, 87
Soler, J. D., Hennebelle, P., Martin, P. G., et al. 2013, ApJ, 774, 128
Sugitani, K., Nakamura, F., Watanabe, M., et al. 2011, ApJ, 734, 63